Physica Scripta



RECEIVED 31 March 2021

REVISED 15 June 2021

ACCEPTED FOR PUBLICATION

23 June 2021

PUBLISHED
2 July 2021

PAPER

Density functional study of the variants of inter-Coulombic decay resonances in the photoionization of $Cl@C_{60}$

Ruma De¹, Esam Ali¹, Steven T Manson² and Himadri S Chakraborty¹

- Department of Natural Sciences, D. L. Hubbard Center for Innovation, Northwest Missouri State University, Maryville, Missouri 64468, United States of America
- ² Department of Physics and Astronomy, Georgia State University, Atlanta, Georgia, United States of America

E-mail: himadri@nwmissouri.edu

Keywords: resonances, photoionizations, DFT, ICD, Endofullerene, Auger-ICD, hybridization

Abstract

Inter-Coulombic decay (ICD) resonances in the photoionization of $Cl@C_{60}$ endofullerene molecule are calculated using a perturbative density functional theory (DFT) method. This is the first ICD study of an open shell atom in a fullerene cage. Three classes of resonances are probed: (i) Cl inner vacancies decaying through C_{60} outer continua, (ii) C_{60} inner vacancies decaying through Cl outer continua, and (iii) inner vacancies of either system decaying through the continua of $Cl-C_{60}$ hybrid levels, the hybrid Auger-ICD resonances. Comparisons with $Ar@C_{60}$ results reveal that the properties of hybrid Auger-ICD resonances are affected by the extent of level hybridization.

1. Introduction

In loosely bound composite matters, such as polymers, liquids, and biological systems, the relaxation of an innershell vacancy resulting in the emission of an outershell electron, both belonging to the same site of the system, is the regular Auger process. But, this vacancy can also decay by transferring excess energy to a neighboring site. This migrated energy can subsequently drive the emission of an electron from that site. Such processes, the inter-Coulombic decay (ICD) [1], are abundant in nature when energetically allowed, unless quenched by a competing process, and piggyback on the long range electron-electron Coulomb interactions. Broadly speaking, the excess energy-transfer to a neighboring site can be triggered via three distinct mechanisms. (i) An outer electron of the vacancy site can itself fill in the vacancy—the regular ICD [2]. (ii) A weakly bound electron from the ionizing neighboring site can transfer and fill the vacancy—the electron transfer mediated decay (ETMD) [3]. (iii) A slow passerby electron can be captured into the vacancy—the inter-Coulombic electron capture (ICEC) [4]. Experimentally, the precursor excitation process to create the vacancy can be induced in varieties of ways: The early work of the observation of ICD in Ne dimers used synchrotron radiation for this purpose [5]. To achieve a higher pulse rate, for instance to carry out time-resolved experiment, free electron laser sources are more appropriate [6]. Furthermore, charged particle impact, such as pulsed electron guns [7] or alpha-particle impact [8] have also been used. ICD signatures are probed by traditional methods of electron [9] and ion [10] spectroscopy, including various coincidence techniques [11]. Access to time-resolved ICD dynamics has also been possible by the contemporary pump-probe approaches [6, 12], specifically, by light field streaking techniques [13]. A recent comprehensive review of the experimental and theoretical research of the ICD topic, including the range of materials studied and potential applications, can be found in [14]. Very recently, the measurement of ICD in liquid water is reported which draws interesting comparisons with ICD in water clusters [15].

Probing ICD processes in relatively simpler vapor-phase materials is of considerable spectroscopic interest [16–20]. One class of such systems of current theoretical and experimental study is endofullerene complexes, in which an atomic or a small molecular host is placed in a fullerene cage. These are unique heterogeneous, nested dimers of weak host-fullerene bonding. From the experimental side, the synthesis techniques for these materials are fast-developing [21] with an advantage of their room-temperature stability. Furthermore, these materials are

Phys. Scr. **96** (2021) 104007

relevant in a number of applied contexts [22]. And, note that measurements of a strong ICD signal in a molecular endofullerene, $Ho_3N@C_{80}$, has recently been reported [23].

If the electron that creates the vacancy subsequently fills the hole to release energy, the process is conventionally called the *participant* ICD. The first *ab initio* calculations of participant ICD induced resonances in the photoionization of C_{60} levels induced by Ar inner 3s [24] and Kr inner 4s [25] vacancy decays, the atom-to-fullerene ICD, were performed by our group. Later we also studied ICD resonances in the reverse process of fullerene-to-atom decay [26]. In addition, a remarkable coherence between the Auger and ICD amplitudes to produce a novel class of resonances in the photoionization of atom-fullerene hybridized states was also predicted [24, 25]. However, these studies cover only close-shell confined atoms. On the other hand, consideration of open-shell atomic endofullerenes to access their ICD properties arouses particular interest given their recent photoresponse studies [27, 28]. In general, due to the existence of unpaired electrons, there are attractive fundamental interests in such systems. These include long spin relaxation times in N@ C_{60} [29] while enhancement and diminution in hyperfine coupling, respectively, in P@ C_{60} [30] and exotic muonium@ C_{60} [31]. In this article, therefore, a prototypical openshell system of Cl@ C_{60} has been considered for the first time to capture its ICD processes along the photoionization route. A comparison with the results of Ar@ C_{60} , the nearest close-shell system of Cl@ C_{60} , exposes the role of atom- C_{60} hybridization in the Auger-ICD coherence process.

2. A fleeting description of theory

Kohn–Sham density functional theory (DFT) is used to describe the ground, photoexcited, and photoionized electronic properties of Cl@C₆₀ [27]. The C₆₀ molecule is modeled by smudging sixty C⁴⁺ ions over a classical spherical jellium shell, fixed in space, with an experimentally known C₆₀ mean radius of 3.5Å and thickness Δ . The nucleus of a Cl atom is placed at the center of the sphere. The Kohn–Sham equations for the system of a total of 240 + N electrons (N = 17 for Cl and 240 delocalized electrons from C₆₀) are then solved to obtain the ground state properties in DFT. The gradient-corrected Leeuwen and Baerends exchange-correlation (XC) functional [LB94] [32] is used for the accurate asymptotic behavior of the ground state radial potential

$$V_{\rm DFT}(\mathbf{r}) = V_{\rm jel}(\mathbf{r}) - \frac{z_{\rm atom}}{r} + \int d\mathbf{r}' \frac{\rho(\mathbf{r}')}{|\mathbf{r} - \mathbf{r}'|} + V_{\rm XC}[\rho(\mathbf{r})], \tag{1}$$

which is solved self-consistently in a mean-field framework. The requirement of charge neutrality produced Δ = 1.3 Å, in agreement with the value inferred from experiment [33, 34]. We note that, unlike Hartree–Fock type methods that treats the non-local exchange exactly, DFT models as in the current study can use adjustable parameters of the functional to force accurate ground state properties even for general open-shell systems [35]. The best parametric optimization was previously obtained [27] to reasonably produce experimental and NIST-based ground state information for Cl. Although the jellium-based DFT potential is a simplification to the atomistic molecular potential of C_{60} , previous calculations based on this model explained photoionization cross section measurements reasonably well [33, 36]. In addition, the present calculations are the only extant treatment of the ICD problem addressed in this paper.

Linear-response time-dependent density functional theory (LR-TDDFT) is employed to simulate the dynamical response of C_{60} to incident photons [36]. The single-electron dipole operator, z, corresponding to light that is linearly polarized in z-direction, induces a frequency-dependent complex change in the electron density arising from dynamical electron correlations. This can be written, using the independent particle (IP) susceptibility χ_0 , as

$$\delta\rho(\mathbf{r};\omega) = \int \chi_0(\mathbf{r},\mathbf{r}';\omega)[z' + \delta V(\mathbf{r}';\omega)]d\mathbf{r}',$$
(2)

in which

$$\delta V(\mathbf{r};\,\omega) = \int \frac{\delta \rho(\mathbf{r}';\,\omega)}{|\mathbf{r} - \mathbf{r}'|} d\mathbf{r}' + \left[\frac{\partial V_{xc}}{\partial \rho} \right]_{\rho = \rho_0} \delta \rho(\mathbf{r};\,\omega),\tag{3}$$

where the first and second terms on the right hand side are, respectively, the induced changes of the Coulomb and the exchange-correlation potentials. Obviously, δV includes the dynamical field produced by important electron correlations within the linear response regime. In this method, the photoionization cross section corresponding to a bound-to-continuum dipole transition $n\ell \to k\ell'$ is given by

$$\sigma_{n\ell \to k\ell'} \sim |\mathcal{M}|^2 = |\langle k\ell'|z + \delta V|n\ell\rangle|^2,\tag{4}$$

where, in the LR-TDDFT matrix element \mathcal{M} , $\mathcal{D} = \langle k\ell'|z|n\ell \rangle$ and $\langle k\ell'|\delta V|n\ell \rangle$ are, respectively, the IP and correlation matrix elements. For the convenience of notation, we use the symbol $n\ell$ to denote pure levels of the confined Cl atom and @ $n\ell$ to represent pure levels of the doped C₆₀.

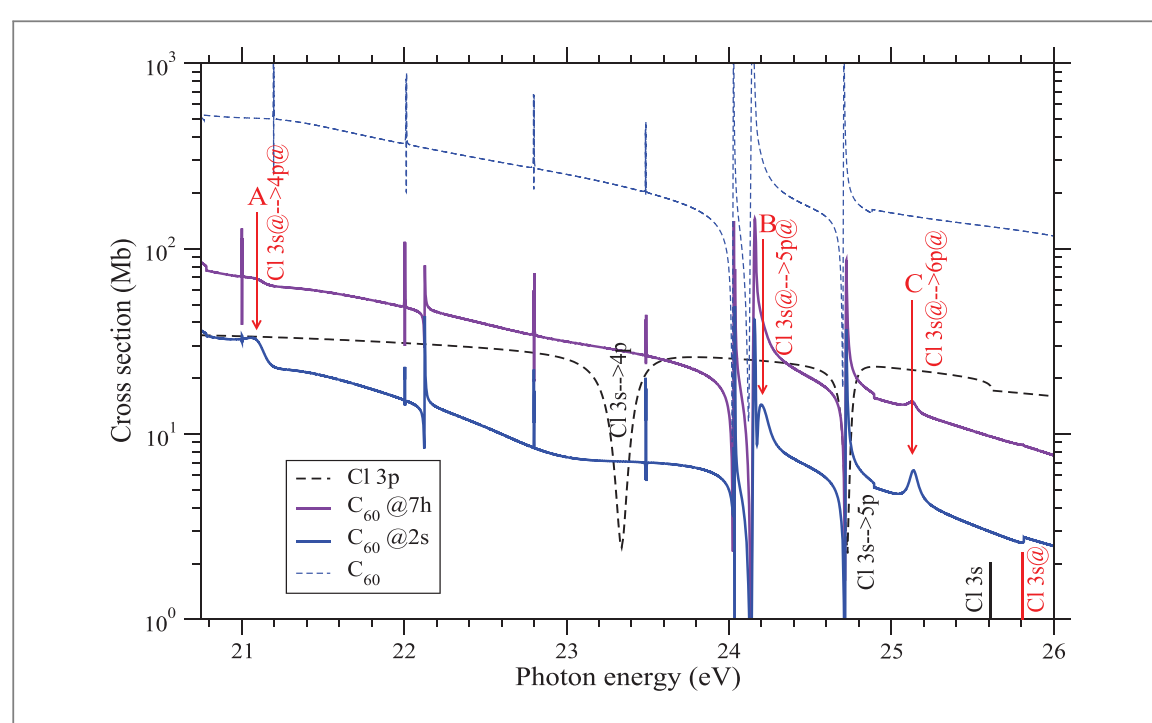


Figure 1. (Color online) Photoionization cross sections of free Cl 3p and empty C_{60} (total) compared with the results for C_{60} @7h and @2s levels in Cl@ C_{60} . Three Cl-to- C_{60} ICD resonances (labeled as A,B,C) are identified in the C_{60} @7h and @2s cross sections which can be compared with regular Auger resonances in free Cl 3p.

In general, the full matrix element of photoionization of a level of Cl@C₆₀ can be written as:

$$\mathcal{M}(E) = \mathcal{D}(E) + M^{c-c}(E) + M^{d-c}(E), \tag{5}$$

where M^{c-c} and M^{d-c} are, respectively, contributions from continuum-continuum (c-c) and discrete-continuum (d-c) channel couplings. $\langle k\ell'|\delta V|n\ell\rangle$ in equation (4) accounts for these coupling contributions. M^{c-c} constitutes a rather smooth many-body contribution to nonresonant cross section, while the Auger or ICD resonances originate from M^{d-c} .

3. Results and discussions

3.1. Cl-to-C₆₀ ICD resonances

Using the well-known approach by Fano [37] to describe the dynamical correlation through the interchannel coupling, the amplitude of resonant ICD of Cl inner 3s@ photo-vacancies via C₆₀ @nl ionization can be expressed by M^{d-c} that denotes the coupling of Cl 3s@ $\rightarrow \eta p$ @ discrete excitation channels with the @ $nl \rightarrow kl'$ continuum channel of C₆₀. Following [24], M^{d-c} can thus be written as:

$$M_{@nl}^{\mathrm{d-c}}(E) = \sum_{n} \sum_{l'} \frac{\left\langle \psi_{3s@ \to \eta p@} | \frac{1}{|\mathbf{r}_1 - \mathbf{r}_2|} | \psi_{@nl \to kl'}(E) \right\rangle}{E - E_{3s@ \to \eta p@}} \mathcal{D}_{3s@ \to \eta p@}, \tag{6}$$

where $E_{3s@\to\eta p@}$ and $\mathcal{D}_{3s@\to\eta p@}$ are, respectively, excitation energies and IP matrix elements of channels $3s@\to\eta p@$, and E is the photon energy corresponding to the @nl transition to continuum. In equation (6) the ψ are IP wavefunctions that represent the final states (channels) for transitions to excited ηp or continuum kl states. Obviously, the Coulomb coupling matrix element in the numerator of equation (6) acts as the passageway for energy transfer from the Cl de-excitation across to the C_{60} ionization process, producing ICD resonances in the C_{60} @nl cross sections.

Three such Cl-to- C_{60} ICD resonances, corresponding to Cl $3s@ \to \eta p@$ with $\eta = 4, 5, 6$ (labeled as A, B and C), are seen in C_{60} @7h (HOMO) and C_{60} @2s cross sections in figure 1. Note that these resonance features in @2s are more prominent due to relatively smaller values of non-resonant background of the @2s cross section. Also shown are the corresponding Auger resonances in free Cl 3p cross section from the decay of the first two 3s excitations which show clear Fano window-shape (also seen in experiments [38]), due to the higher background 3p continuum transition strength. In comparison, the corresponding ICD resonances show dramatically different, small, peak-type shapes, indicating lower continuum transition strengths. They also show the expected energy red-shifts, owing to the smaller binding energy of confined Cl 3s@. These Cl-to- C_{60} ICD resonances are qualitatively similar to those of Ar-to- C_{60} found earlier [24], albeit with expected energy offsets. The remaining

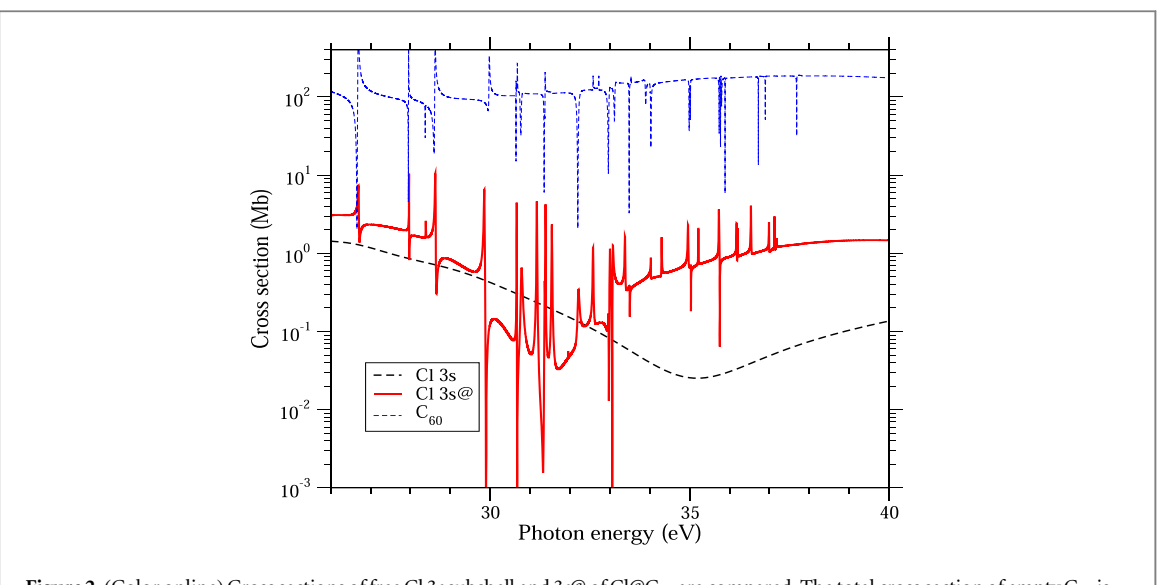


Figure 2. (Color online) Cross sections of free Cl 3s subshell and 3s@ of Cl@ C_{60} are compared. The total cross section of empty C_{60} is also presented.

resonances in @7h and @2s cross sections in figure 1 are from Auger decays of C_{60} inner holes and are almost stable in their energies as can be seen by comparing with the empty C_{60} total cross section (shown).

3.2. C₆₀-to-Cl ICD resonances

A coupled-channel representation of the matrix element like equation (6), but to address the ICD resonances from the decay of C_{60} inner excitations that appear in the Cl $3s@ \rightarrow kp$ photoionization of Cl@ C_{60} , can be written as,

$$M_{3s@}^{\mathbf{d}-\mathbf{c}}(E) = \sum_{@n\ell} \sum_{\eta\lambda} \frac{\left\langle \psi_{@n\ell \to @\eta\lambda} | \frac{1}{|\mathbf{r}_1 - \mathbf{r}_2|} | \psi_{3s@ \to kp}(E) \right\rangle}{E - E_{@n\ell \to \eta\lambda}} \mathcal{D}_{@n\ell \to @\eta\lambda}. \tag{7}$$

Since a number of inner C_{60} vacancies can be produced that are degenerate with Cl 3s@ ionization, two sums have been introduced.

 C_{60} -to-Cl ICD resonances are displayed in figure 2 for 3s@ photoionization of Cl. Note that the cross section is highly structured with the resonances when compared to the smooth 3s cross section of free Cl (shown). As seen, the free Cl result in the current energy range does not include any regular Auger decay of atomic innershell vacancies, indicating that the ICD process completely dominates the vacancy decay. The resonances are strong and of varied shapes. Their narrow width owes to the C_{60} excitations. Indeed, C_{60} wavefunctions, atypical of cluster properties, are delocalized, spreading over a large volume (see figure 3). Since the autionization rate involves the matrix element of $1/r_{12}$ [equation (7)], spread-out wavefunctions translate to a decrease in the value of the matrix elements.

figure 2 also shows that for Cl 3s@ the Cooper minimum, seen in the non-resonant background values of the curve, moves lower in energy to about 32 eV from its positions of 35 eV in free Cl. This shift is a consequence of the atom- C_{60} dynamical coupling of Cl $ns@ \rightarrow kp$ ionization channel with a host of C_{60} continuum channels and was earlier noted for confined Ar and Kr as well [26]. This coupling is included in M^{c-c} in equation (5). A comparison with the resonances (Auger) in the empty C_{60} cross section (shown) indicates a general energy correspondence between Auger and ICD features, although there appear a rather dramatic shape alterations, in particular, at higher energies. The overall behavior of the ICD resonances is found very similar to the previous results for Ar 3s@ and Kr 4s@ caged in C_{60} .

3.3. Hybrid Auger-ICD resonances

About an equal share of mixing in ground state hybridization between valence 3p orbital for Ar with C_{60} 3p was earlier found in Ar@ C_{60} [24]. In fact, the hybridization gap of 1.52eV between symmetrically (Ar+ C_{60}) and antisymmetrically (Ar $-C_{60}$) mixed hybrid levels in that earlier calculation was in good agreement with the measured value of 1.6 \pm 0.2 eV [39]. This hybridization in Cl@ C_{60} , which is similar to the bonding and antibonding states in molecules or dimers, can be written as,

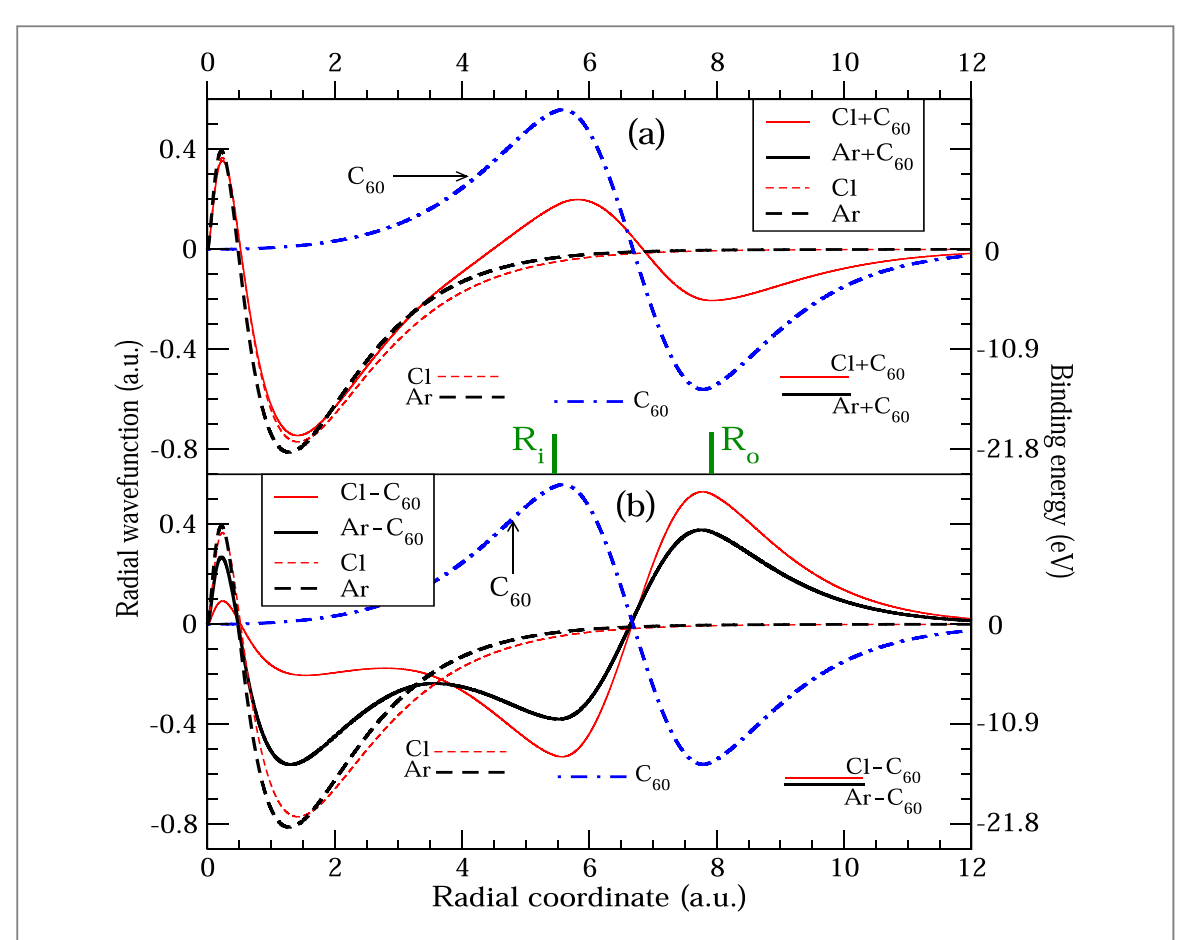


Figure 3. (Color online) Radial symmetric (a) and antisymmetric (b) wavefunctions of $Cl@C_{60}$ versus $Ar@C_{60}$. Wavefunctions of participant levels of free systems are displayed. Relevant binding energies in eV (scaled in opposite *y*-axis) are also graphed. The inner (R_i) and outer (R_o) radii of the C_{60} shell are shown on panel (a). Reproduced from [27]. © IOP Publishing Ltd. All rights reserved.

$$Cl3p \pm C_{60}3p = |\phi_{\pm}\rangle = \sqrt{\alpha} |\phi_{3pCl}\rangle \pm \sqrt{1 - \alpha} |\phi_{3pC_{60}}\rangle.$$
 (8)

Both free and hybrid radial wavefunctions and corresponding energies are shown in figure 3 for a comparison between $Cl@C_{60}$ and $Ar@C_{60}$ ground state properties. Figure 3 clearly shows somewhat weakened hybridization in $Cl@C_{60}$ versus $Ar@C_{60}$ which is primarily due to higher $Cl\ 3p$ binding energy leading to a larger energy gap between this level with $C_{60}\ 3p$. We note that recent DFT structure calculations using atomistic description of C_{60} predict hybridization of the confined atom's p level with C_{60} in similar proportions of mixing [40].

Following equation (8), the hybridization of the continuum channels assumes the form

$$|\psi_{\pm}\rangle = \sqrt{\alpha} |\psi_{3p@Cl \to ks,d}\rangle \pm \sqrt{1 - \alpha} |\psi_{@3pC_{60} \to ks,d}\rangle, \tag{9}$$

where $\psi_{3p@Cl\to ks,d}$ and $\psi_{@3pC_{60}\to ks,d}$ are the wavefunctions of the channels. Using equation (9) and recognizing that the overlap between a pure Cl and a pure C_{60} bound state is negligible (see figure 3), we may separate the atomic and fullerene regions of integration to write the matrix elements M^{d-c} for emissions from hybrid levels as

$$M_{\pm}^{\mathrm{d-c}}(E) = \sum_{n\ell} \sum_{\eta\lambda} \left[\sqrt{\alpha} \frac{\left\langle \psi_{n\ell \to \eta\lambda} | \frac{1}{|\mathbf{r}_{\pm} - \mathbf{r}_{n\ell}|} | \psi_{3p@\mathrm{Cl} \to ks, d}(E) \right\rangle}{E - E_{n\ell \to \eta\lambda}} \right]$$

$$\pm \sqrt{1 - \alpha} \frac{\left\langle \psi_{n\ell \to \eta\lambda} | \frac{1}{|\mathbf{r}_{\pm} - \mathbf{r}_{n\ell}|} | \psi_{@3p\mathrm{C}_{60} \to ks, d}(E) \right\rangle}{E - E_{n\ell \to \eta\lambda}} \right] \mathcal{D}_{n\ell \to \eta\lambda}.$$

$$(10)$$

It is now straightforward to understand from equation (10) that if the inner vacancy corresponding to $n\ell\to\eta\lambda$ is located at Cl, then the first term in equation (10) denotes the decay through the Cl continuum, like in the Auger decay, and the second term will embody the decay through the C₆₀ continuum, like the ICD. This will result in resonant hybrid Auger-ICD (RHA-ICD) features from coherence in a hybrid level cross section driven by a Cl hole. These resonances for both hybrid levels of Cl@C₆₀ are presented in the top panel of figure 4 and labeled as A, B and C for three $3s@\to np@$ excitations. On the other hand, the original vacancy at C₆₀ in

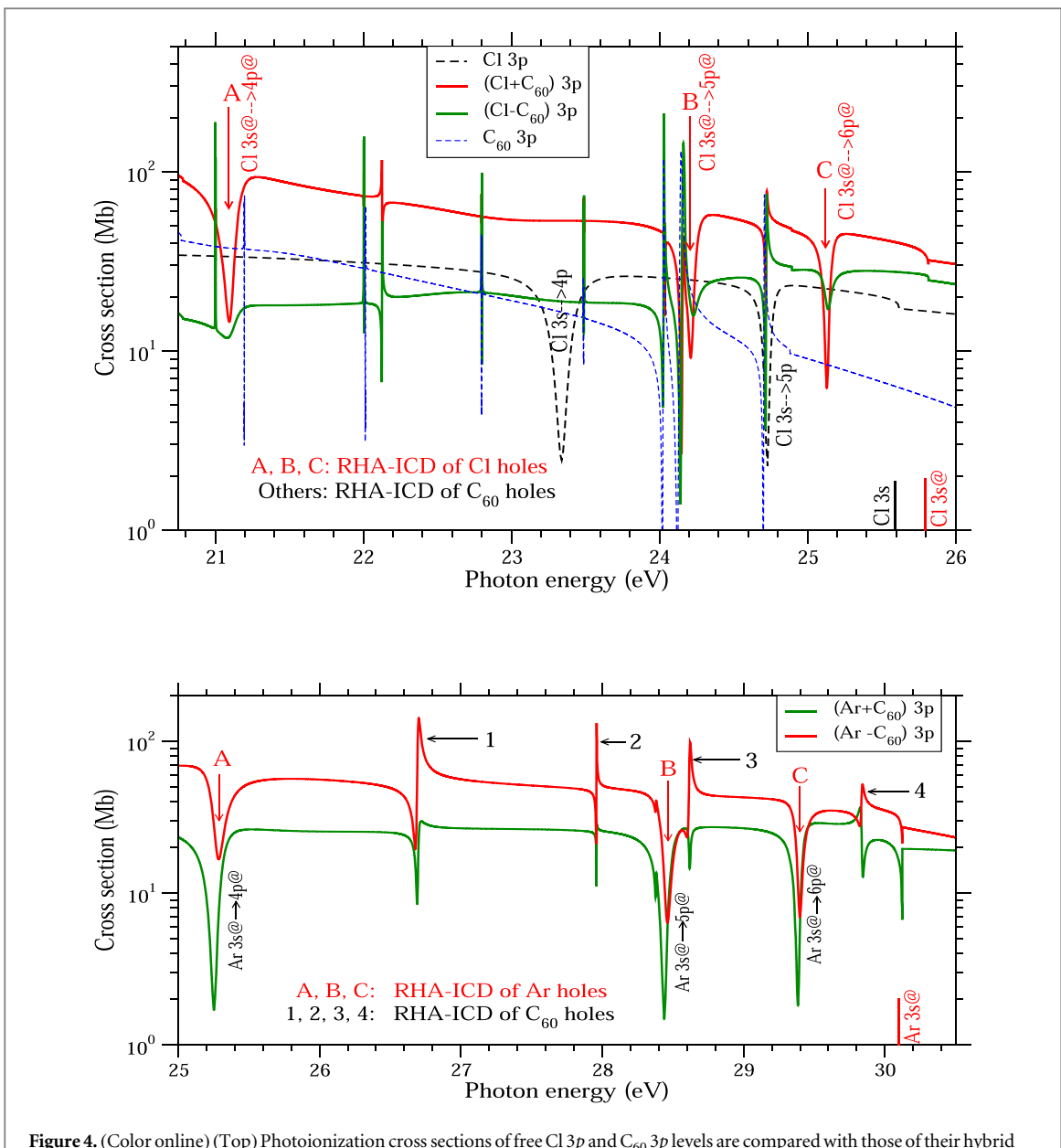


Figure 4. (Color online) (Top) Photoionization cross sections of free Cl 3p and C_{60} 3p levels are compared with those of their hybrid pair. (Bottom) Published [24] Ar@ C_{60} results for hybrid levels.

equation (10) will produce coherent RHA-ICD features initiated by a C_{60} hole. All remaining resonances in figure 4 (top) for hybrid states are from this latter category. We note in figure 4 (top) that the resonances A-C in both $Cl \pm C_{60}$ 3p cross sections feature window-type shapes, like the free Cl Auger resonances (shown), generally suggesting strong continuum transitions. These RHA-ICD window resonances may likely be observed in the experiment due to their broad widths. However, we further note that these resonance shapes are significantly stronger for the symmetric $Cl + C_{60}$ level. The generic shapes of RHA-ICD structures from C_{60} hole-decays, on the other hand, are seen to be non-window type, while they are substantially more prominent in the antisymmetric $Cl - C_{60}$ emission. The cause of these disparities is discussed below.

The novel RHA-ICD features were originally predicted for $Ar@C_{60}$ [24] that are also presented in figure 4 (bottom) to draw insights from comparisons. As seen for $Ar@C_{60}$, for each hybrid level cross section these resonances initiated by creation of Ar inner 3s holes (A-C) versus by creation of C_{60} inner holes (1-4) are of approximately similar strengths. This is a direct consequence of a similar degree of mixing between Ar and C_{60} characters in $Ar \pm C_{60}$ levels (see figure 3)—a fact that generates similar magnitudes of overlaps in the Coulomb coupling matrix elements in equation (10). However, as noted before, the mixing reduces in $Cl@C_{60}$. As seen in figure 3, while the $Cl + C_{60}$ level contains more Cl character, $Cl - C_{60}$ has more C_{60} character. This fact, through the coupling matrix elements in equation (10), translates into stronger RHA-ICD structures, A-C, for the decay of Cl holes in $Cl + C_{60}$ than in $Cl - C_{60}$. Likewise, this same fact is also responsible for the opposite behavior for C_{60} hole decay, that is, the corresponding stronger structures in $Cl - C_{60}$ versus in $Cl + C_{60}$.

3.4. ETMD admixture

In an endofullerene system the excited state for the precursor excitation resulting in an Auger decay or an ICD can itself be a state which is a hybrid of an atomic and a C_{60} excited state of same angular momentum character. Here the excited states in question include $\eta p@,@\eta\lambda$ and $\eta\lambda$ in, respectively, equation (6), (7) and (10). This suggests that the part of the excited probability that will transfer to the other system can fall back in to the vacancy to initiate a resonant Auger decay or an ICD or a hybridized Auger-ICD. Furthermore, a very careful comparison between the ICD related results with corresponding empty C_{60} results in figures. 2 and 4 reveals a very few extra resonances in the ICD curves. These are present owing to the additional excited states in the spectrum of the whole compound, since it now also includes the empty states of the caged atom that can be transfer-excited by a C_{60} electron. This clearly suggests that some of the resonances of both ICD and Auger nature presented here may incorporate coherent mixing with ETMD amplitudes. Of course, these contributions are hard to separate. A detailed discussion about such coherent combination of resonant ICD and ETMD mechanisms, but for a specific case of C_{60} -to-Ar ICD, was given elsewhere [26].

4. Conclusion

We present results of various kinds of single-electron ICD-type resonances in the photoemission of the $Cl@C_{60}$ molecule. This is the first ICD study of an endofullerene with a one-vacancy, open-shell atom inside. The calculation is carried out in a jellium-based linear-response time-dependent density functional framework that has previous success. The study includes resonant decays of Cl (C₆₀) innershell excitation vacancies degenerate with C_{60} (Cl) outershell ionization vacancies. A uniquely different class of resonant features decaying into atomfullerene hybrid final state vacancies has also been presented which arises from the interference of the Auger channel with an intrinsically connected ICD channel. These resonances are found to be remarkably strong, and the ones initiated by atomic excitations are quite broad. Hence they are likely experimentally measurable, allowing a powerful access to ICD dynamics. Furthermore, the hybridized character of some of the excited states of the compound points to a coherence of ICD with the ETMD process. Such ICD-ETMD coherence should be abundant—all it would require is that both the fullerene and the trapped atom or molecule have dipole-allowed excited states of the same (angular momentum) symmetry so they can hybridize. We further emphasize that the present calculation only includes participant RICDs where the precursor hole is filled by the excited electron itself. However, it is of great interest to access the influence of spectator processes where a different electron occupies the hole likely significantly affecting the situation. Based upon our explanation of the details of multicenter decay, the resonant ICD predicted here is expected to be a strong process in general for any atom or molecule encaged in any fullerene, in any position, central or not.

By freezing the molecular vibrations, the present jellium calculation effectively models the stuation at 0K sample temperature. A finite sample temperature in an experiment can, therefore, potentially wash out some of the narrow resonances due to the lattice vibration driven broadening. Yet, as pointed above, the Cl-based features, such as, Cl-to- C_{60} ICD resonances (Figure 1) and RHA-ICD of Cl holes (Figure 4), may still be detectable due to their larger widths, drawn from the width of measured window resonances of isolated Cl (like Ar) [38]. Beyond this, the colder the target temperature, the more detailed of the ICD signals that can be accessed. Besides encouraging experiments on $Cl@C_{60}$, or even $Ar@C_{60}$, the other aim of this study is to motivate more sophisticated treatments of the current problem.

Finally, with the contemporary focus [41] on photoemission phase and time delay studies by interferometric metrology [42], particularly at Fano window resonances for free Ar [43], we hope that the current results will stimulate similar ultrafast spectroscopic studies of ICD resonances in fullerene confined atoms. And to that end, our future research outlook includes investigations of Wigner type intrinsic time delays of these various resonant ICD emissions.

Acknowledgments

The work is supported by the National Science Foundation grant PHY-1806206 and the US Department of Energy, Office of Science, Basic Energy Sciences under Grant No. DE-FG02-03ER15428.

Data availability statement

All data that support the findings of this study are included within the article (and any supplementary files) or can be obtained by directly requesting the authors.

ORCID iDs

References

- [1] Cederbaum L S, Zobeley J and Tarantelli F 1997 Giant intermolecular decay and fragmentation of clusters Phys. Rev. Lett. 79 4778
- [2] Ouchi T et al 2011 Three-electron interatomic Coulombic decay from the inner-valence double-vacancy states in NeAr Phys. Rev. Lett. 107 053401
- [3] Förstel M, Mucke M, Arion T, Bradshaw A M and Hergenhahn U 2011 Autoionization mediated by electron transfer Phys. Rev. Lett. 106 033402
- [4] Sisourat N, Miteva T, Gorfinkiel J D, Gokhberg K and Cederbaum L S 2018 Interatomic Coulombic electron capture from first principles *Phys. Rev.* A **98** 020701(R)
- [5] Jahnke T et al 2004 Experimental observation of interatomic Coulombic decay in neon dimers Phys. Rev. Lett. 93 163401
- [6] Schnorr K et al 2013 Time-resolved measurement of interatomic Coulombic decay in Ne₂ Phys. Rev. Lett. 111 093402
- [7] Yan Set al 2018 Interatomic relaxation processes induced in neon dimers by electron-impact ionization Phys. Rev. A 97 010701(R)
- [8] Kim H-K et al 2011 Enhanced production of low energy electrons by alpha particle impact Proc. Natl. Acad. Sci. USA 108 11821
- [9] Marburger S, Kugeler O, Hergenhahn U and Möller T 2003 Experimental evidence for interatomic coulombic decay in Ne clusters Phys. Rev. Lett. 90 203401
- [10] Wiegandt F et al 2019 Direct observation of interatomic Coulombic decay and subsequent ion-atom scattering in helium nanodroplets Phys. Rev. A 100 022707
- [11] LaForge A C, Shcherbinin M, Stienkemeier F, Richter R, Moshammer R, Pfeifer T and Mudrich M 2019 Highly efficient double ionization of mixed alkali dimers by intermolecular Coulombic decay Nat. Phys. 15 247
- [12] Takanashi T et al 2017 Time-resolved measurement of interatomic Coulombic decay induced by two-photon double excitation of Ne_2 Phys. Rev. Lett. 118 033202
- [13] Trinter F et al 2013 Evolution of interatomic Coulombic decay in the time domain Phys. Rev. Lett. 111 093401
- [14] Jahnke T et al 2020 Interatomic and intermolecular Coulombic decay Chem. Rev. 120 11295
- [15] Zhang P, Perry C, Luu T T, Matselyukh D and Wörner H J 2021 Observation of intermolecular Coulombic decay in liquid water arXiv:2103.15014
- [16] Barth S, Joshi S, Marbuger S, Ulrich V, Lindblad A, Öhrwall G, Bjömeholm O and Hergenhahn U 2005 Observation of resonant Interatomic Coulombic Decay in Ne clusters J. Chem. Phys. 122 241102
- [17] Aoto T, Ito K, Hikosaka Y, Shigemasa E, Penent F and Lablanquie P 2006 Properties of resonant interatomic Coulombic decay in Ne dimers Phys. Rev. Lett. 97 243401
- [18] Kim H-K et al 2013 Ion-impact-induced interatomic Coulombic decay in neon and argon dimers Phys. Rev. A 88 042707
- [19] Trinter F et al 2013 Vibrationally resolved decay width of interatomic Coulombic decay in HeNe Phys. Rev. Lett. 111 233004
- [20] Najjari B, Voitkiv A B and Müller C 2010 Two-center resonant photoionization Phys. Rev. Lett. 105 153002
- [21] Popov A A, Yang S and Dunsch L 2013 Endohedral fullerenes Chem. Rev. 113 5989
- [22] Popov A A 2017 Synthesis and molecular structures of endohedral fullerenes *Endohedral Fullerenes*: *Electron Transfer and Spin* (*Nanostructure Science and Technology Series*) ed A A Popov (Cham: Springer)
- [23] Obaid R et al 2020 Intermolecular Coulombic decay in endohedral fullerene at the $4d \rightarrow 4f$ resonance Phys. Rev. Lett. 124 113002
- [24] Javani M H, Wise J B, De R, Madjet M E, Manson S T and Chakraborty H S 2014 Resonant Auger-intersite-Coulombic hybridized decay in the photoionization of endohedral fullerenes *Phys. Rev.* A **89** 063420
- [25] Magrakvelidze M, De R, Javani M H, Madjet M E, Manson S T and Chakraborty H S 2016 Coherence of Auger and inter-Coulombic decay processes in the photoionization of Ar@C₆₀ versus Kr@C₆₀ Eur. Phys. J. D 70 96
- [26] De R, Magrakvelidze M, Madjet M E, Manson S T and Chakraborty H S 2016 First prediction of inter-Coulombic decay of C₆₀ inner vacancies through the continuum of confined atoms *J. Phys.* B 48 11LT01
- [27] Shields D, De R, Madjet M E, Manson S T and Chakraborty H S 2020 Photoemission from hybrid states of Cl@C₆₀ before and after a stabilizing charge transfer *J. Phys.* B **53** 125101
- [28] Shields D, De R, Ali E, Madjet M E, Manson S T and Chakraborty H S 2020 A density functional theory based comparative study of hybrid photoemissions from $Cl@C_{60}$ Br@ C_{60} and $I@C_{60}$ Eur. Phys. J. D 74 191
- [29] Morton J J L, Tyryshkin A M, Ardavan A, Porfyrakis K, Lyon S A and Briggs G A D 2007 Environmental effects on electron spin relaxation in N@C₆₀ Phys. Rev. B 76 085418
- [30] Knapp C, Weiden N, Kass H, Dinse K-P, Pietzak B, Waiblinger M and Weidinger A 1998 Electron paramagnetic resonance study of atomic phosphorus encapsulated in [60] fullerene *Mol. Phys.* 95 999 online (2011)
- [31] Donzelli O, Briere T and Das T P 1996 Location of muonium and hydrogen in C60 fullerene and associated electronic structure and hyperfine properties *Hyperfine Interact.* 97 19
- [32] van Leeuwen R and Baerends E J 1994 Exchange-correlation potential with correct asymptotic behavior Phys. Rev. A 49 2421
- [33] Rüdel A, Hentges R, Becker U, Chakraborty H S, Madjet M E and Rost J M 2002 Imaging Delocalized Electron Clouds: photoionization of C₆₀ in fourier reciprocal space Phys. Rev. Lett. 89 125503
- [34] Magrakvelidze M, Anstine D M, Dixit G, Madjet M E and Chakraborty H S 2015 Attosecond structures from the molecular cavity in fullerene photoemission time delay Phys. Rev. A 91 053407
- [35] Anderson L N, Bele'en Oviedo M and Wong B W 2017 Accurate electron affinities and orbital energies of anions from a nonempirically tuned range-separated density functional theory approach J. Chem. Theory Comput. 13 1656
- [36] Choi J, Chang E H, Anstine D M, Madjet M E and Chakraborty H S 2017 Effects of exchange-correlation potentials on the density-functional description of C_{60} versus C_{240} Phys. Rev. A 95 023404
- [37] Fano U 1961 Effects of configuration interaction on intensities and phase shifts Phys. Rev. 124 1866
- [38] van der Meulen P, Krauset MO, Caldwell CD, Whitfield SB and de Lange CA 1991 Autoionization resonances in atomic chlorine: the 3s3p⁵(³P ⁰_{2,1,0})np Rydberg series *J. Phys.* B 24 L573

[39] Morscher M, Seitsonen AP, Ito S, Takagi H, Dragoe N and Greber T 2010 Strong $3p - T_{1u}$ hybridization in Ar@C₆₀ Phys. Rev. A 82 051201(R)

- [40] Madjet M E, Ali E, Carignano M, Vendrell O and Chakraborty H S 2021 Ultrafast transfer and transient entrapment of photoexcited Mg electron in Mg@ C_{60} Phys. Rev. Lett. 126 183002
- [41] Dixit G, Chakraborty H S and Madjet M E 2013 Time Delay in the Recoiling Valence Photoemission of Ar Endohedrally Confined in C_{60} Phys. Rev. Lett. 111 203003
- [42] Kotur M et al 2016 Spectral phase measurement of a Fano resonance using tunable attosecond pulses Nature Comm. 7 10566
- [43] Cirelli C et al 2018 Anisotropic photoemission time delays close to a Fano resonance Nature Comm. 9 955